551.551.2 : 551.554

On wind and shear stress profiles above a change in surface roughness

By P. A. TAYLOR
Department of Mathematics, University of Toronto

(Manuscript received 18 March 1968; in revised form 30 July 1968)

SUMMARY

The problem of determining the distribution of velocity and shear stress in the flow above a surface with an abrupt change in roughness is considered by using the 'mixing-length' theory to relate the shear stress to the velocity profile and solving the resulting system of partial differential equations numerically. The results are compared with those obtained by Panofsky and Townsend (1964) and Taylor (1967), by assuming special forms for the velocity or shear stress profiles.

NOTATION

$d(x)$	height of internal boundary layer
F, F^*	functions in shear stress distributions
k	von Kármán's constant ($= 0{\cdot}4$)
l	mixing length
l_s	length scale for self-preserving flow
m	ratio of downstream to upstream roughness lengths ($= z_1/z_0$)
M	roughness change parameter $\left(= \ln \frac{z_0}{z_1}\right)$
$S(x)$	surface friction velocity parameter $\left(= \frac{u_0 - u_1(x)}{u_0}\right)$
$u_0, u_1(x)$	surface friction velocities for $x < 0$, $x \geqslant 0$
U, W	velocity components in x and z directions
x	horizontal distance downwind of roughness change
z	vertical height
z_0, z_1	roughness lengths for $x < 0$, $x \geqslant 0$
δ	internal boundary layer thickness
τ, τ_0	horizontal kinematic shear stress and surface value
η	scaled vertical height ($= z/d$)
ζ	logarithmic vertical scale $\left(= \ln \frac{z + z_1}{z_1}\right)$
Primes	denote non-dimensionalized quantities; e.g. U', x'. The non-dimensionalization is with respect to u_0 and z_1.

Some of the above notation is shown schematically in Fig. 1

1. INTRODUCTION

Elliott (1958), Panofsky and Townsend (1964), and Taylor (1967) have considered the effect of an abrupt change in surface roughness on the airflow close to the ground under conditions of neutral thermal stability. The basic aim of these papers has been to describe the flow downstream of a roughness change, the change taking place across a line perpendicular to the mean wind direction. Upstream of the roughness change the flow is assumed to be in equilibrium with the underlying surface and is assumed to have a kinematic shear stress independent of height ($= u_0^2$) and a logarithmic velocity profile of the form

$$U = \frac{u_0}{k} \ln \frac{z + z_0}{z_0}, \qquad (1)$$

where z_0 is the upstream roughness length and k is von Kármán's constant.

Some experimental observations of this flow situation have been made and are described in Munn (1966, p. 109) whilst others are now under way. Panofsky and Townsend give some comparisons between theoretical and experimental velocity profiles but these are rather inconclusive, the main factor being that velocity variations are relatively small and insensitive. Shear stress values would provide a much better comparison.

The present paper considers the same flow situation but uses numerical solution of the partial differential equations describing the flow instead of assuming special forms for shear stress or velocity profiles within an internal boundary layer.

2. Description of previous theories

In addition to the usual boundary layer approximations and neglect of the viscous terms in the momentum equation the work of Elliott, Panofsky and Townsend and Taylor is based on the hypothesis that the effect of the roughness change is confined to an ' internal boundary layer ' of height $d(x)$ within which the velocity profile may be represented by an assumed form. It is the assumed form for velocity profile that varies in the three theories. Above the internal boundary layer the kinematic shear stress is assumed to retain its original upstream value (u_0^2) whilst the new value of surface kinematic shear stress, which will be a function of x, is denoted by $u_1^2(x)$. The assumed form for velocity profile within the internal boundary layer is substituted into the momentum equation which is then integrated across the layer to give one relationship between $d(x)$ and $u_1(x)$. The requirement that the velocity is continuous at the outer edge of the interval boundary layer provides a second relation and the resulting differential equations may then be solved to give the downstream variation of $d(x)$, $u_1(x)$ and, subsequently, the velocity profile. Although it is not essential, and I am most grateful to one of the referees for pointing this out, the earlier theories have also made the assumption that the velocity and shear stress profiles are related by the equation

$$\tau^{1/2} = k(z + z_l)\frac{\partial U}{\partial z} \qquad (2)$$

where z_l is the local value of the roughness length. This has the value z_0 for $x < 0$ and z_1 for $x \geqslant 0$. Eq. (2) could be considered as a ' mixing-length ' relation

$$\tau^{1/2} = l\,\frac{\partial U}{\partial z}$$

where l, the mixing-length is given by

$$l = k(z + z_l) \qquad (3)$$

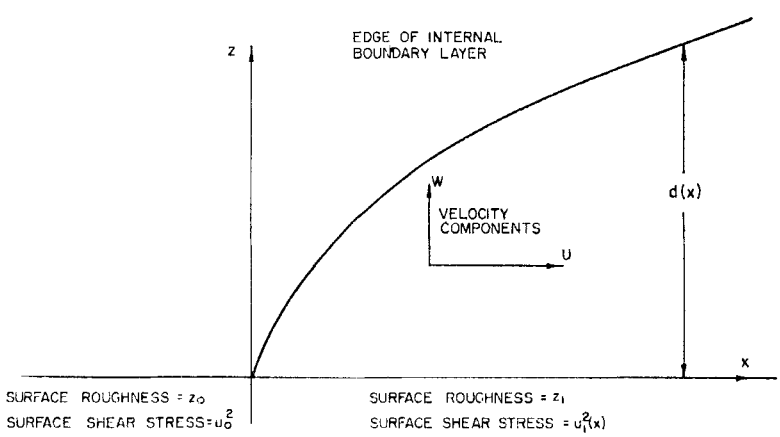

Figure 1. Schematic representation of the internal boundary layer.

If these relations are assumed to hold within the internal boundary layer the assumed forms for velocity profile give rise to equivalent forms for the shear stress profiles.

The comparison between the three theories is clearest in terms of the resulting vertical distribution of (kinematic shear stress)$^{\frac{1}{2}}$. Using the notation

$$S(x) = \frac{u_0 - u_1(x)}{u_0} \quad . \quad . \quad . \quad . \quad . \quad (4)$$

the distributions of shear stress assumed within the internal boundary layer are

Elliott: $$\tau^{1/2} = u_0(1 - S) = u_1(x) \quad . \quad . \quad . \quad . \quad (5)$$

Panofsky and Townsend: $$\tau^{1/2} = u_0[(1 - S) + S\eta], \quad \text{where } \eta = \frac{z}{d}$$

$$= u_1 - (u_1 - u_0)\eta \quad . \quad . \quad . \quad . \quad (6)$$

Taylor: $$\tau^{1/2} = u_0[(1 - S) + S(10\eta^3 - 15\eta^4 + 6\eta^5)] \quad . \quad (7)$$

Eq. (7) is based on an application of the von Kármán-Pohlhausen technique using the highest order polynomial that will permit the reduction of the problem to a single ordinary differential equation.

A comparison of these three forms is given in Fig. 2. It should be borne in mind that $d(x)$ and $u_1(x)$ will be different in final solutions to the three cases.

Although the downstream variation in velocity profiles and surface shear stress may be obtained from the previous theories without recourse to the mixing length or a similar hypothesis the cross-stream distribution of shear stress cannot be obtained without its use. In this sense the mixing-length hypothesis, or some similar closure of the governing system of equations, is essential in order to be able to find a solution to the problem.

The hypotheses concerning the velocity profile within the internal boundary layer are, however, basically a mathematical simplification leading to an approximate solution along the lines of the von Kármán-Pohlhausen technique (see for example Goldstein 1938, p. 158). An alternative to using these assumed profiles is to perform a numerical solution of the governing partial differential equations. Results from this approach are

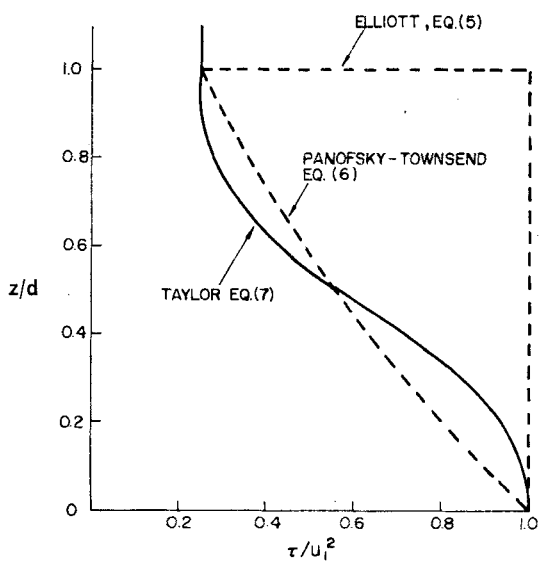

Figure 2. Comparison of shear stress forms with $S = -1$.

presented here and compared with earlier results to test how accurate the previous theories have been in giving the solution to the boundary layer equations used. The question of the validity or approximate validity of the mixing length hypothesis is a separate matter but there are good reasons for supposing that its use will at least give approximately correct solutions. The real test will be from direct measurements of shear stress and wind shear within the internal boundary layer, whilst comparison of experimental results with numerical solutions obtained by methods such as those described here will be useful in determining whether the predictions and hypotheses are approximately correct.

3. Equations and method of solution

Using the notation given at the beginning of the paper and schematically in Fig. 1, the equations governing the flow are:

The x-momentum equation

$$U\frac{\partial U}{\partial x}+W\frac{\partial U}{\partial z}=\frac{\partial \tau}{\partial z}. \qquad (8)$$

The continuity equation

$$\frac{\partial U}{\partial x}+\frac{\partial W}{\partial z}=0. \qquad (9)$$

These equations, together with Eq. (2), form a parabolic system which may be solved, in theory at least, with the boundary and initial conditions

$$U=\frac{u_0}{k}\ln\frac{z+z_0}{z_0},\quad W=0 \quad \text{on} \quad x=0.$$

$$U=W=0 \quad \text{on} \quad z=0,\quad x\geqslant 0.$$

$$\tau\to u_0^2 \quad \text{as} \quad z\to\infty.$$

We may non-dimensionalize these equations with respect to u_0 and z_1, introduce $\zeta=\ln(z/z_1+1)$ and eliminate τ to give

$$U'\frac{\partial U'}{\partial x'}+W'e^{-\zeta}\frac{\partial U'}{\partial \zeta}=2k^2e^{-\zeta}\left(\frac{\partial U'}{\partial \zeta}\right)\left(\frac{\partial^2 U'}{\partial \zeta^2}\right) \qquad (10)$$

$$\frac{\partial U'}{\partial x'}+e^{-\zeta}\frac{\partial W'}{\partial \zeta}=0 \qquad (11)$$

where

$$U'=\frac{U}{u_0},\quad W'=\frac{W}{u_0},\quad x'=\frac{x}{z_1} \quad \text{and} \quad z'=\frac{z}{z_1}.$$

The initial condition now becomes

$$U'=\frac{l}{k}\ln(mz'+1) \quad \text{on} \quad x'=0 \qquad (12)$$

where $m=z_1/z_0$. We will also use the notation $M=\ln(z_0/z_1)$ for comparison with previous theories.

The method used to obtain numerical solutions to the problem was basically the standard one of replacing the ζ derivatives by finite differences to give a system of ordinary differential equations for dU_i'/dx, where U_i' is the x-component of velocity at a fixed

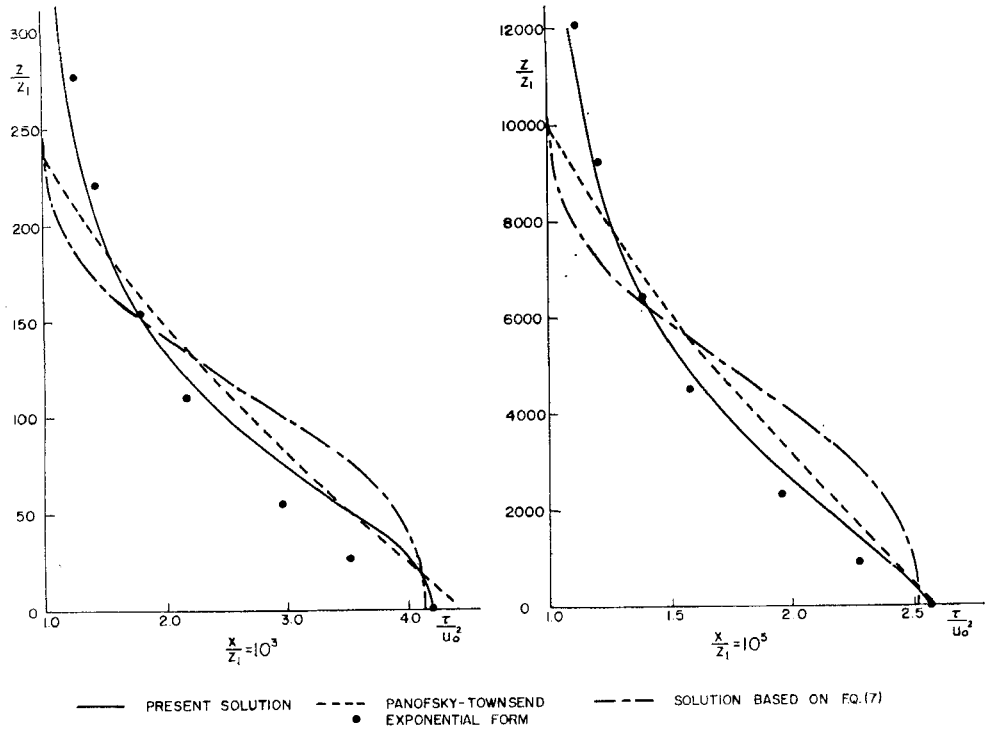

Figure 3. Shear stress profiles, $M = -5$.

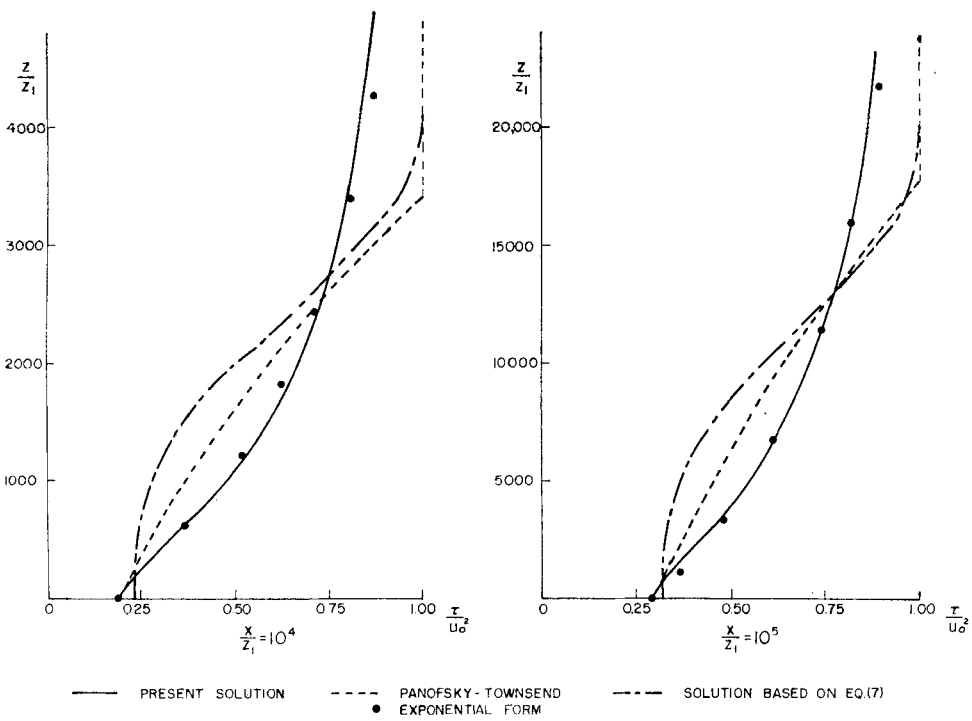

Figure 4. Shear stress profiles, $M = +4$.

vertical height. These equations for the dU_i/dx were then solved numerically using a version of the Runge-Kutta method in standard use on the University of Toronto's IBM 7094 computer. Details of the finite difference equations and the operation of the method are given in an Appendix. Checks were made using finer grid spacings and higher accuracy criteria to test the accuracy of the solutions in some test cases and the results to be given are estimated to be within 1 per cent of the exact solutions of the differential equations.

In any comparison between the results obtained by this method and experimental results, the usual inaccuracies inherent in the boundary layer approximation will occur for small x. In addition the fact that we are taking $l = k(z + z_0)$ when $x > 0$ and $l = k(z + z_1)$ when $x > 0$, for all z, will expose an inadequacy of the theory at small x for heights of the same order of magnitude as the roughness lengths. At any given height the local effective value of surface roughness should perhaps start off as z_0 at $x = 0$ and gradually change to z_1 as the effects of the roughness change diffuse out into the flow. For large heights the value is unimportant whilst for small heights the change may be expected to take place quite rapidly but the assumption of an abrupt change at $x = 0$ will produce some erroneous results in the region close to the roughness change.

These errors are due to the way in which the problem is set up rather than any method of solution and for the heights and downstream distances of practical interest will be negligible.

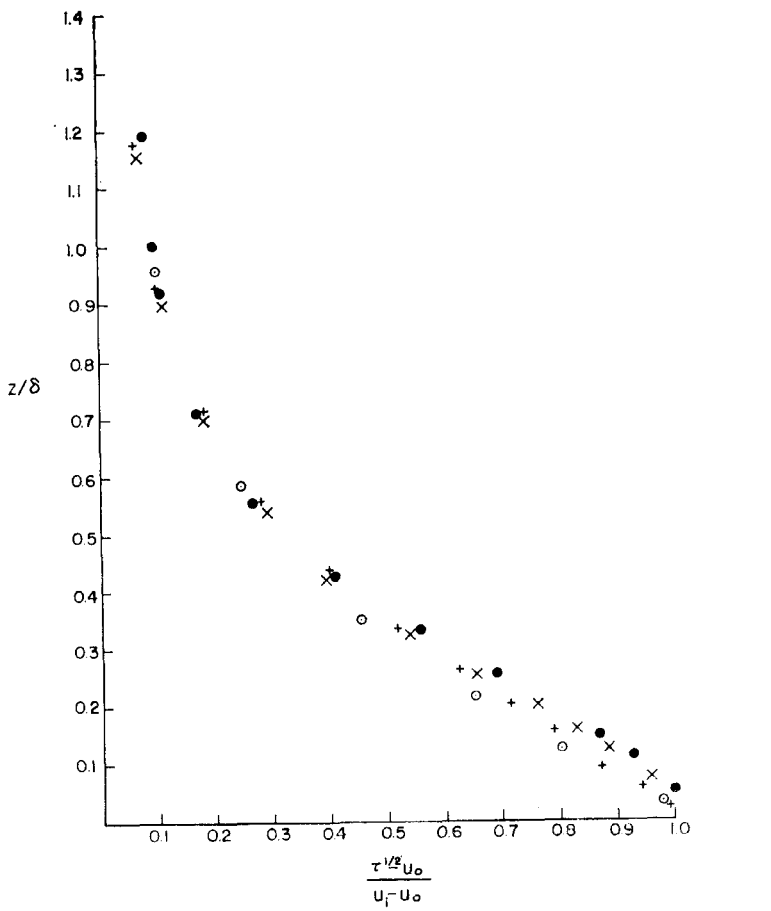

Figure 5. Self-preservation of shear stress distribution $M = -2$.

4. Comparison of results with other theories

Numerical results for velocity and shear stress have been obtained for a range of values of M, both positive, corresponding to flow from a relatively rough to a relatively smooth surface and negative corresponding to smooth to rough flow. Inasmuch as the present approach predicts the vertical variation in shear stress, whereas earlier theories make assumptions which may be considered as essentially equivalent to this, it seems appropriate to consider the shear stress profiles as a basis for comparison. We can do this by considering the profiles of τ (or $\tau^{1/2}$) against z (using values for $d(x)$ and $u_1(x)$ calculated using the appropriate theory) as is done in Figs. 3 and 4.

These and similar results show that the Panofsky-Townsend distribution (Eq. (6)) is considerably better than that given by Eq. (7), or the Elliott form (Eq. (5)), and gives shear stress profiles to within about 20 per cent of the finite difference solutions at sufficiently large downstream distances. The error in terms of $\tau^{1/2}$ will be about 10 per cent. The fact that results are closer for $M = -5$ than $M = +4$ is probably due to the relative values of x/z_0 in the two cases; the further downstream we go the closer the present numerical solution and the Panofsky-Townsend solution become. In the results shown the greatest differences occur for $M = +4$ at $x/z_1 = 10^4$. This corresponds to $x/z_0 = 200$ and an internal boundary layer thickness of about 3,500 z_1 or 70 z_0. Whilst this is perhaps

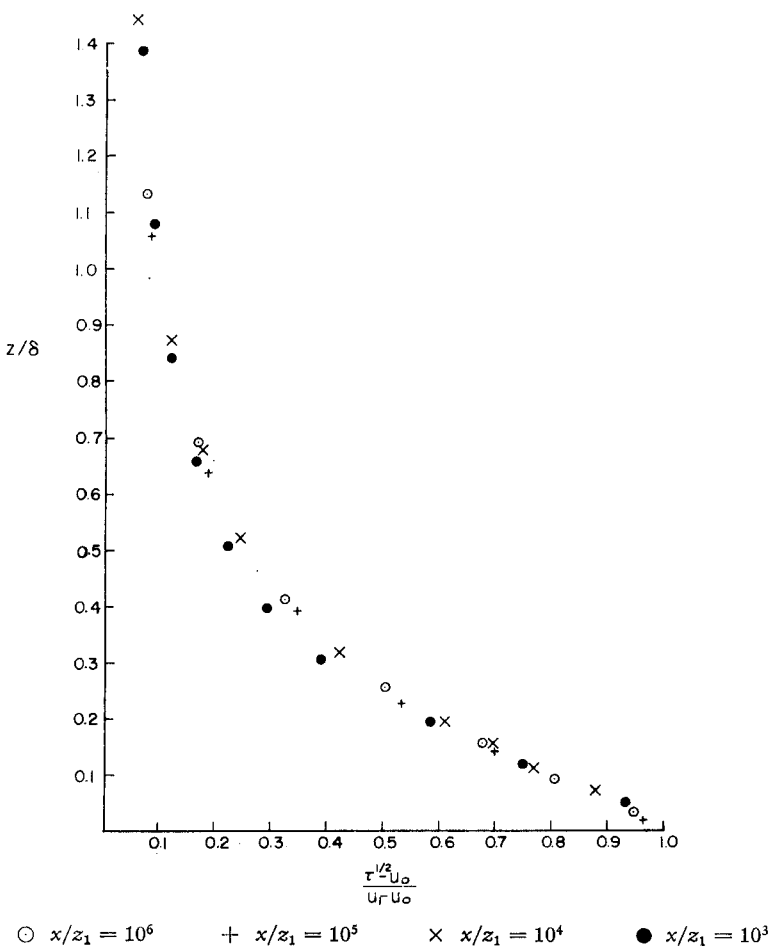

Figure 6. Self-preservation of shear stress distribution $M = +2$.

a borderline case in terms of the complete elimination of the type of error discussed at the end of Section 3, the profiles are quite similar at $x/z_1 = 10^5$ and the differences may be significant in any comparison of theory and experiment.

Alternately we may define an internal boundary layer thickness which can be calculated from the numerical solutions. The boundary layer thickness chosen, which we denote by δ, is the height at which the difference $(\tau^{1/2} - u_0)$ had been reduced to 10 per cent of its value at the surface, i.e. $(u_1 - u_0)$. This height will have unrealistic values for small x where it is of the same order of magnitude as the roughness lengths but once it is greater than the larger of, say, $10^2\, z_0$ and $10^2\, z_1$ it will provide a sensible estimate of the internal boundary layer thickness. Figs. 5 and 6 show $(\tau^{1/2} - u_0)/(u_1 - u_0)$ plotted against z/δ at different downstream distances for $M = -2$ and $M = +2$. It can be seen that the profiles of $\tau^{\frac{1}{2}}$ are very nearly self-preserving in form and could be represented, at least in the lower half of the layer, by a linear variation such as that assumed by Panofsky and Townsend.

We may also compare the shear stress results with the analysis made by Townsend (1965, 1966) on the basis that the flow in the internal boundary layer will be approximately self-preserving. The self-preserving form for shear stress that he proposes is

$$\tau - u_0^2 = (\tau_0 - u_0^2)\, F\left(\frac{z}{l_s}\right) \quad . \quad . \quad . \quad . \quad (13)$$

where l_s is a length scale of the self-preserving process. It should be noted that this is different from the self-preserving forms associated with the Elliott, Panofsky-Townsend and Eq. (7) theories which are of the form:

$$\tau^{1/2} - u_0 = (\tau_0^{1/2} - u_0)\, F^*\left(\frac{z}{l_s}\right). \quad . \quad . \quad . \quad (14)$$

The self-preserving theory is developed in detail by Townsend for small changes in friction velocity and in the case of large negative values of M. The assumption of self-preservation in conjunction with the mixing-length hypothesis predicts an exponential form for F, i.e.

$$F\left(\frac{z}{l_s}\right) = \exp\left(-\frac{z}{l_s}\right) \quad . \quad . \quad . \quad . \quad . \quad (15)$$

The theory is, however, unable to predict l_s or the surface shear stress accurately in the cases of moderate roughness change which are considered here. The resulting form

$$\tau - u_0^2 = (\tau_0 - u_0^2) \exp\left(-\frac{z}{l_s}\right) \quad . \quad . \quad . \quad (16)$$

is shown in Figs. 3 and 4 with an l_s obtained by matching the profiles at the point where $(\tau - u_0^2)$ had fallen to one quarter of its value at the surface. It can be seen that the shapes of the profiles obtained numerically are close to the exponential form predicted by Townsend except for the case of $M = -5$, $x/z_1 = 10^3$. Here better agreement could be obtained by using a higher value of τ_0 in Eq. (16) than that predicted by the numerical solution.

Figs. 7 and 8 show the downstream variation in surface shear stress parameter S predicted by Panofsky and Townsend, Eq. (7) and the present solution. The Panofsky-Townsend results are based on their values for d given in Fig. 1 of their paper with S calculated from their approximate relation

$$S\left(\ln\frac{d}{z_1} - 1\right) = M \quad . \quad . \quad . \quad . \quad . \quad (17)$$

Use of the corresponding exact relation makes very little difference to the results.

Once again differences between the present results and those based on the Panofsky-Townsend theory are small and get smaller as x increases. The same is true of the velocity profile results shown in Figs. 9 and 10. Again the variations between theories are greatest in the rough to smooth flow case.

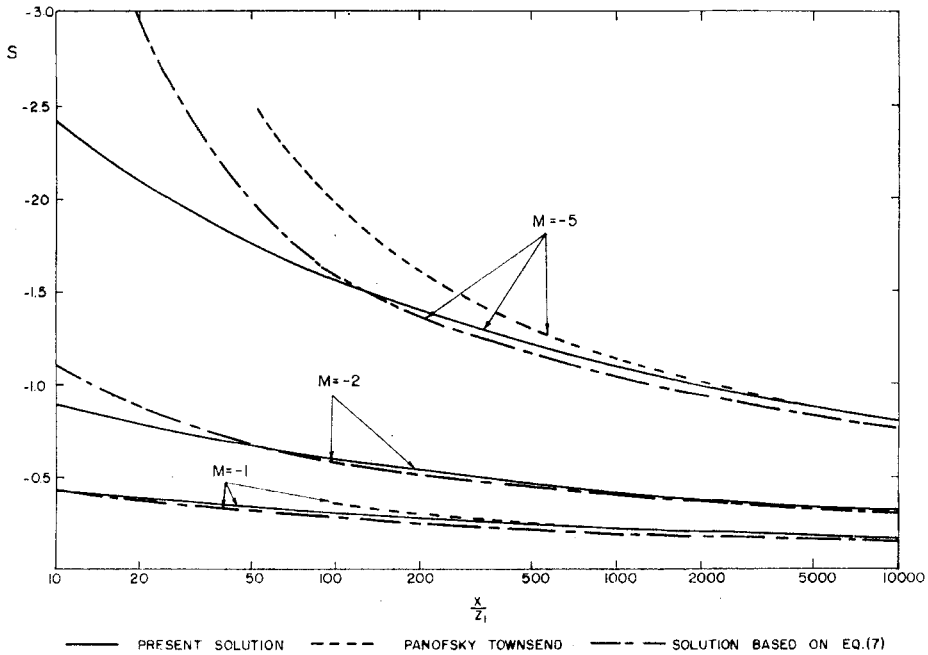

Figure 7. Surface shear stress parameter for smooth-rough flows.

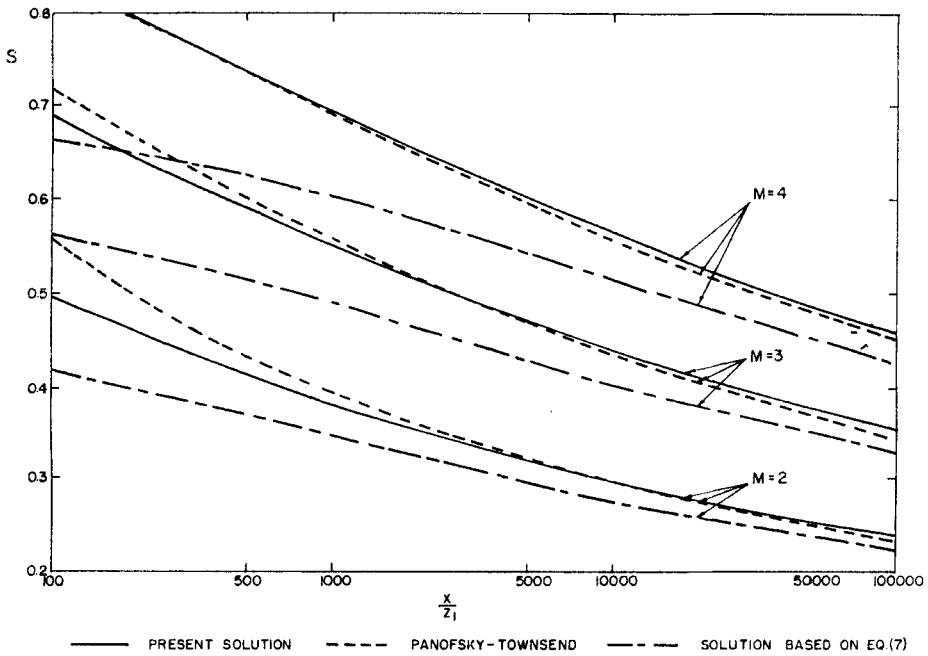

Figure 8. Surface shear stress parameter for rough-smooth flows.

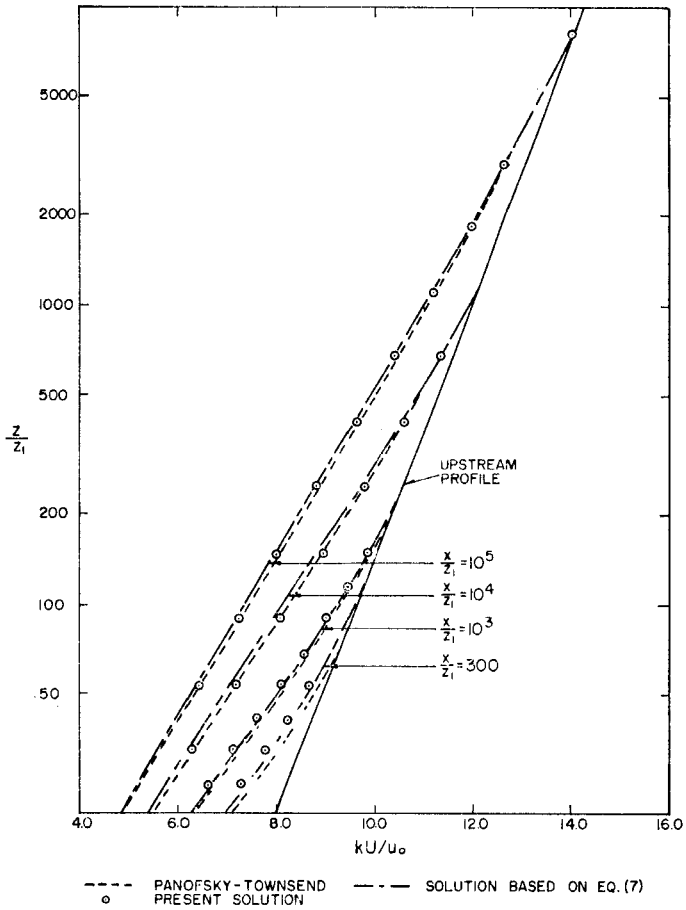

Figure 9. Theoretical wind profiles, $M = -5$.

The results for thickness of the internal boundary layer, characterized by δ are similar to the results given by Panofsky and Townsend. Fig. 11 shows the variation of δ with x given by the present solutions.

5. Conclusions

The principal conclusion is that of the three hypotheses concerning the distribution of shear stress in an internal boundary layer that proposed by Panofsky and Townsend (Eq. (6)) is the most accurate in describing the solutions to Eqs. (8), (9) and (2), and if such a method is required, will give quite good results. The availability of high speed digital computers does, however, mean that the methods used in this paper are quite practical for solving problems such as these, the average time taken for a solution from $x' = 0$ to $x' = 10^6$ being about 8 minutes on an IBM 7094 computer system.

The shape of the shear stress profile given by Townsend's (1965, 1966) theory of self preservation is in good agreement with the results obtained here but the predictions of surface shear stress and internal boundary layer thickness given by the self-preservation theory are only applicable in the case of small roughness changes. It may be possible to develop a theory along the lines of the Elliott and Panofsky-Townsend theories using an exponential form but unless a large number of calculations were required it would have no advantage over the numerical techniques used here.

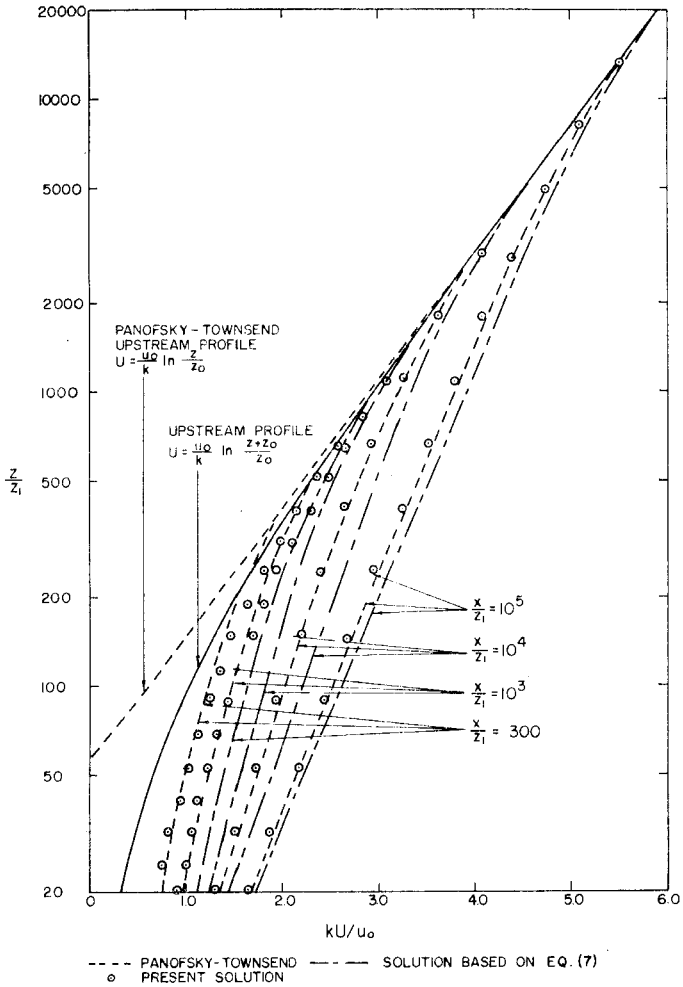

Figure 10. Theoretical wind profiles, $M = 4$.

The fundamental problem remains that of the applicability of the mixing length hypothesis to this type of flow. Change of roughness flows do perhaps provide one of the most interesting applications of this type of semi-empirical theory. If we restrict our consideration for the moment to flows above a change of roughness in cases where the upstream flow is non-developing (e.g. pipe or channel flow, the logarithmic boundary layer discussed, or the atmospheric wind spiral) we may use the observed values of shear stress and velocity profile in the upstream equilibrium flow to determine a form for the mixing length. This we may expect to be of the form

$$l(z_0, z) = kz_0 + f(z) \quad . \quad . \quad . \quad . \quad (14)$$

where, at least in the first 3 cases given as examples, the form of f does not appear to depend on z_0, and will thus be the same in the final downstream steady state. (Experimental results for mixing length distributions in a two-dimensional channel are given by Taylor (1967). The results given for pipes and channels by Nikuradse (1929, 1933), some of which are reproduced in Goldstein (1938, p. 357) and Schlichting (1960, Fig. 20.6) are incorrect near the centre-line of the channel). Simply by altering z_0 at the roughness

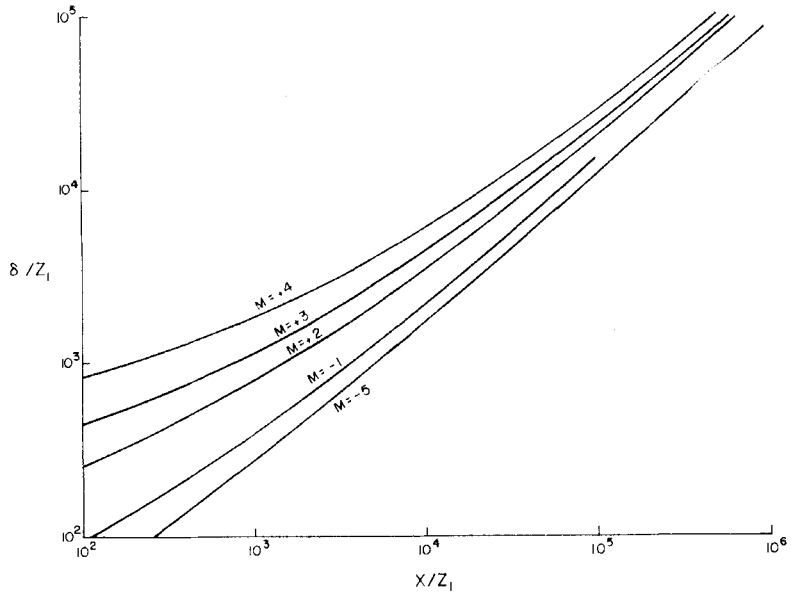

Figure 11. Internal boundary layer thickness, δ.

change we obtain results for the downstream variations in velocity and shear stress profiles which are at least qualitatively correct and will probably be sufficiently accurate for most purposes. Whilst this approach does little to further our understanding of the basic mechanisms of turbulent flow it does provide a means of describing a flow situation which is of considerable interest to micrometeorologists, even if their main concern is simply to avoid it.

Acknowledgments

The results based on Eq. (7) formed part of the author's investigations whilst a research student at the University of Bristol and supported by a Central Electricity Research Laboratory contract. The author would like to record his gratitude to Dr. A. R. Paterson of the Mathematics Department, University of Bristol for his advice and encouragement.

References

Elliott, W. P. 1958 'The growth of the atmospheric Internal Boundary Layer,' *Trans. Amer. Geophys. Union*, **39**, pp. 1,048-1,054.

Goldstein, S. 1938 *Modern developments in fluid dynamics*, Clarendon Press, Oxford.

Munn, R. E. 1966 *Descriptive micrometeorology*, Academic Press, New York.

Nikuradse, J. 1929 'Untersuchungen über die Strömungen des Wassers in konvergenten und divergenten Kanälen,' V.D.I. Forschungsarb. 289.

1933 'Strömungsgesetze in rauhen Rohren' Forschungsheft 361 (Translated into English as NACA TM 1,292).

Panofsky, H. A. and Townsend, A. A. 1964 'Change of terrain roughness and the wind profile,' *Quart. J. R. Met. Soc.*, **90**, pp. 147-155.

Schlichting, H. 1960 *Boundary layer theory* (4th edition), McGraw-Hill, New York.

Taylor, P. A. 1967 'On turbulent wall flows above a change in surface roughness,' University of Bristol Ph.D. Thesis (unpublished).

Townsend, A. A. 1965 'Self-preserving flow inside a turbulent boundary layer,' *J. Fluid Mech.*, **22**, pp. 773-797.

1966 'The flow in a turbulent boundary layer after a change in surface roughness,' *Ibid.*, **26**, pp. 255-266.

Appendix

Details of numerical method

The basis of the method used to solve Eqs. (10) and (11) is to replace the ζ derivatives by finite differences, to give a set of ordinary differential equations with x as the independent variable and dependent variables U_j, where U_j is the value of U' at a fixed value of $\zeta\,(=\zeta_j)$. We thus obtain U_j along a series of lines $\zeta = \zeta_j$. These lines were equally spaced along the ζ axis and central finite difference approximations, correct to order h^2, (where h is the line spacing) were obtained.

The finite differences used to replace $\partial U/\partial\zeta$, $\partial^2 U/\partial\zeta^2$ in Eq. (10) are

$$\left(\frac{\partial U}{\partial \zeta}\right)_{\zeta=\zeta_j} = \frac{U_{j+1} - U_{j-1}}{2h} \quad . \quad . \quad . \quad . \quad \text{(A1)}$$

$$\left(\frac{\partial^2 U}{\partial \zeta^2}\right)_{\zeta=\zeta_j} = \frac{U_{j+1} - 2U_j - U_{j-1}}{h^2} \quad . \quad . \quad . \quad \text{(A2)}$$

Eq. (11) may be used to give W_j in terms of W_{j-1}, dU_j/dx, dU_{j-1}/dx, by using finite differences centred on a point midway between ζ_j and ζ_{j-1}. This gives

$$W_j = W_{j-1} - \frac{h}{2} e^{\zeta_j - \frac{h}{2}} \left(\frac{dU_j}{dx} + \frac{dU_{j-1}}{dx}\right). \quad . \quad . \quad \text{(A3)}$$

Substituting for W_j from this equation and for the ζ-derivatives from (A1) and (A2) into Eq. (10) now gives the result

$$\frac{dU_j}{dx} = \frac{\left[\frac{k^2 e^{-\zeta_j}}{h^3}(U_{j+1} - U_{j-1})(U_{j+1} - 2U_j + U_{j-1}) + \left(\frac{1}{4} e^{-\frac{h}{2}} \frac{dU_{j-1}}{dx} - \frac{1}{2h} e^{-\zeta_j} W_{j-1}\right)(U_{j+1} - U_{j-1})\right]}{\left[U_j - \frac{1}{4} e^{-\frac{h}{2}}(U_{j+1} - U_{j-1})\right]} \quad . \quad . \quad . \quad . \quad \text{(A4)}$$

Using Eqs. (A4) and (A3) we could now start out at the ground (ζ_0) where $W_0 = 0$ and $dU_0/dx = 0$ and work out one step at a time to determine dU_j/dx for $j = 1, 2, \ldots, N$ given U_j for $j = 0, 1, \ldots, N + 1$ and in this way integrate downstream. The additional value U_{N+1} required at each step being given by the outer boundary condition that $\tau = u_0^2$, thus

$$U_{N+1} = U_N + \frac{l}{k} \ln\left(\frac{mz_{N+1} + 1}{mz_N + 1}\right) \quad . \quad . \quad . \quad \text{(A5)}$$

where z_N is the value of z' corresponding to $\zeta = \zeta_N = Nh$.

The problem of numerical stability associated with this type of problem usually gives rise to a condition that the downstream steplength (i.e. the stepsize used in the numerical solution of the equations for dU_j/dx) must be less than some function of the cross-stream stepsize or line spacing – frequently some factor multiplied by the square of the cross-stream spacing. Now in the problem considered here it is the cross-stream spacing of z as against ζ that appears to govern the stability and hence the ζ-line spacing close to the wall that governs the maximum downstream stepsize compatible with numerical stability. In order to increase the downstream stepsize and reduce computing time we

may increase the effective z-spacing at the wall by assuming a logarithmic velocity profile of the form

$$U = \frac{u_1(x)}{k} \ln\left(\frac{z + z_1}{z_1}\right) \quad . \quad . \quad . \quad . \quad . \quad (A6)$$

for $\zeta \leqslant \zeta_I$, where ζ_I is chosen to correspond to one of the original lines ($\zeta = Ih$). This gives rise to some modification of the equation for dU_I/dx which is now the starting point for the evaluation of the remaining cases of Eq. (A4).

In non-dimensional form (A6) becomes

$$U' = \frac{u_1'}{k}\zeta.$$

So

$$U_I = \frac{u_1'}{k}\zeta_I. \quad . \quad . \quad . \quad . \quad . \quad . \quad (A7)$$

Now the continuity Eq. (11) gives, on integration from 0 to ζ_I,

$$W_I = -\frac{l}{k}\frac{du_1'}{dx}[(\zeta_I - 1)e^{\zeta_I} + 1],$$

or

$$W_I = -\frac{[(\zeta_I - 1)e^{\zeta_I} + 1]}{\zeta_I}\frac{dU_I}{dx} \quad . \quad . \quad . \quad . \quad (A8)$$

This we may substitute into Eq. (10) along with the finite difference approximations to give

$$\frac{dU_I}{dx} = \frac{\dfrac{k^2 e^{-\zeta_I}}{h^3}(U_{I+1} - 2U_I + U_{I-1})(U_{I+1} - U_{I-1})}{[U_I - Ae^{-\zeta_I}(U_{I+1} - U_{I-1})/2h]}, \quad . \quad (A9)$$

where $A = [(\zeta_I - 1)e^{\zeta_I} + 1]/\zeta_I$,

and $U_{I-1} = ((\zeta_I - h)/\zeta_I)\,U_I$, corresponding to the value given by Eq. (A6).

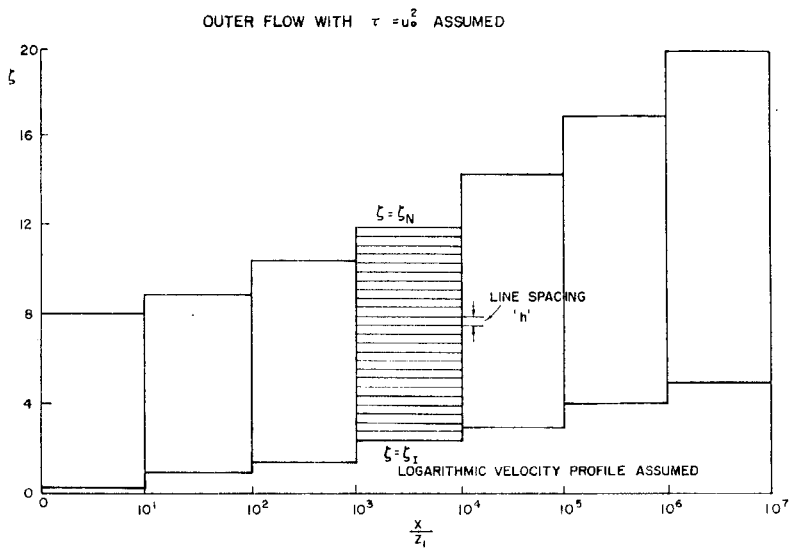

Figure A1. Numerical solution scheme.

TABLE A1. PARAMETERS USED IN NUMERICAL SOLUTIONS

	h	ζ_I	$z' I$	ζ_N	$z' N$
$x = 0 \rightarrow 10$	0·125	0·25	0·28	6	4×10^2
$x = 10 \rightarrow 10^2$	0·125	1·0	1·7	7	1×10^3
$x = 10^2 \rightarrow 10^3$	0·25	1·5	3·5	8·25	$3{\cdot}6 \times 10^3$
$x = 10^3 \rightarrow 10^4$	0·25	2·5	11·2	10	2×10^4
$x = 10^4 \rightarrow 10^5$	0·5	3	19	12·5	$2{\cdot}5 \times 10^5$
$x = 10^5 \rightarrow 10^6$	0·5	5	148	15	3×10^6

We may now use Eq. (A9) to evaluate dU_I/dx, then Eq. (A8) for W_I and then Eqs. (A4), (A3) to evaluate the remaining x derivatives. We treat this scheme as defining a set of first order ordinary differential equations which we may solve from, say, $x = a$ to $x = b$ given suitable initial conditions at $x = a$.

The integration (from $x = 0$ to $x = 10^6$ in most cases) was performed in a series of blocks, from $0 \rightarrow 10$, $10 \rightarrow 10^2$, etc., and the values of I, N and h were altered from block to block to give a solution that was both accurate for low values of x and did not take too much computer time at large x. An increase in N at a block change was achieved by repeated use of Eq. (A5) to give initial values for U' on the ' new ' lines whilst adjustments in h were in the form of a doubling of the line spacing and eliminating the intermediate lines. The system used is shown schematically in Fig. A1 and the values of parameters h, ζ_I, $z' I$, ζ_N, $z' N$ are given in Table A1 for smooth to rough flows. Higher values of N were found necessary for rough to smooth flow cases.

The downstream integration was performed using a modified Runge-Kutta method capable of adjusting its step length to give rapid downstream integration whilst keeping estimated errors below a stipulated maximum. The accuracy parameter used was equivalent to a permitted error in the velocity values (U_r) of approximately 10^{-3} per block. The ability of the method to adjust its own steplength is very useful as it eliminates the need for an involved numerical stability analysis or large number of trials to find the best values for step spacing. The programmes were written in FORTRAN IV and run on the University of Toronto's IBM 7094 computer. The Runge-Kutta method is described by N. F. Stewart (1965), ' An integration subroutine using a Runge-Kutta method,' M.Sc. Thesis, University of Toronto.